Partial spin polarization of conductance in vertical bi-layer nanowire with rectangular and smooth lateral confinement potential

T. Chwiej*
AGH University of Science and Technology, al. A. Mickiewicza 30, 30-059 Cracow, Poland

We simulate the electron transport in vertical bi-layer nanowire which can be fabricated in molecular beam epitaxy process with lateral confinement potential formed by means of cleaved overgrowth or surface oxidization methods giving rectangular and smooth side confinement, respectively. In calculations we take into account interaction between charge carriers using DFT within local spin density approximation. If magnetic field is perpendicular to the wire axis, pseudogaps are opened in energy dispersion relation E(k) what in conjunction with spin Zeeman shift of spin-up and spin-down subbands allows for quite high spin polarization of conductance. We find that in nanowire with rectangular lateral confinement potential, electron density has two maximums localized at wire edges in each layers. This modificates strongly all magnetosubbands giving up to four energy minimums in lowest subband and considerably diminishes widths of pseudogaps what translates into low maximal spin polarization of conductance, not exceeding 40%. This drawback is absent in wire with smooth lateral confinement. However, in order to gain a large spin polarization simultaneous tuning of magnetic field as well as the Fermi energies in both layers of nanowire are required.

PACS numbers: 72.25.Dc,73.21.Hb
Keywords: quantum wire, ballistic transport, spin polarized transport

I. INTRODUCTION

Influence of magnetic field on electron transport in double-nanowire system depends on mutual orientation of magnetic field and wire axis.[1–3] In longitudinal magnetic field i.e. directed parallel to wire axis, the wave functions are compressed in direction being perpendicular to electron motion what changes the tunnel coupling bewteen layers.[1,4] On the other hand, perpendicular magnetic field may mix vertical or lateral modes leading to subbands hybrydization.[5,6] Due to magnetic mixing of wave functions localized in different layers, crossings of subbands in energy dispersion relation E(k) are replaced by avoided corissings. In such case, the pseudogaps are open in energy spectrum what brings severe consequences for conductance depending on quality of nanowire.[5,7,8] If transport layers are vertically stacked in nanowire, one over another, and, tilted magnetic field is applied to a system, then more pseudogaps may appear in energy spectrum since both, inter-layer as well as intra-layer modes mixing are allowed what makes such mixing to be more effective.[8] Recently we have indictated[8] that spin polarization of conductance in bi-layer nanowire may reach up to 60% for moderate Fermi energy when only a few transport channels are open. Those preliminary calculations however have not taken into account an electrostatic interaction between electrons in nanosystem which may have a great impact on electron transport[9–13] and only rectangular shape of lateral confinement was considered.

In this work, we continue our theoretical studies of single electron transport in bi-layer nanowire but now we will mainly focus on spin-polarization of conductance when strong magnetic field is applied perpendicularily to wire axis and electrostatic interactions bewteen electrons are taken into account within local spin density approximation. In our considerations we model two types of side confinement potentials, that is, the lateral barriers will have the rectangular or smooth shapes. First type of confinement can be formed by etching of quantum wire from two-dimensional nanostructure that holds an electron gas confined within two layers and next cleaving its side surfaces. This process[14] removes defects from surfaces and then, after deposition of barrier material on both sides of nanowire gives finally side barriers without surface charge. Cross section of confinement potential of such nanowire resembles rectangular well.[14] Second type of the confinement can be formed by surface oxidization of the nanostructure. Two parallel nanogrooves created during this process may sink up to the depth of 85 nanometers[15] with the width of 50 nanometers.[23] Charge gathered on walls of each nanogrooves forms electrostatic barriers which smoothly deplet electron gas confined in both, the upper and lower wells in wire. This technique is fast and very flexible since it allows for formation of much more complicated patterns of confinement potentials like e.g. laterally coupled two quantum rings[16] or a ring capacitively coupled with quantum point contact.[17] The shape of lateral confinement in nanowire remarkably influence on spatial distribution of electron density in quantum wire and the overall electrostatics in nanosystem. Thus, it has a strong impact on single electron transport properties.[18,19]

We found that two edge wells are formed in wire when lateral confinement has rectangular shape. Maxima of electron density are localized in edge wells in each layers what considerably modificates magnetosubbands. For that reason, widths of pseudogaps are substantially reduced and spin polarization of conductance does not exceed 40%, provided that, the width of nanowire equals few tens of nanometers. However, if lateral confinement is smooth, the electron densities in both layers have sin-

gle elongated maximums and neighbouring magnetosubbands are well separated on energy scale. The results of our simulations show that an accidental overlapping of spin-up and spin-down energy branches can decrease maximal value of conductance polarization but we think it can be increased if both, the magnetic field and Fermi energy will simultaneously be tuned.

Paper is organized as follows. In Sec.II we will present details of theoretical model that was used in calculations, an influence of rectangular and smooth lateral confinement potentials on magnetosubbands and spin polarization of conductance of bi-layer nanowire is presented and disscused in Sec.III A and in Sec.III B, respectively. Section IV includes conclusions.

II. THEORETICAL MODEL

A. Model of nanostructure

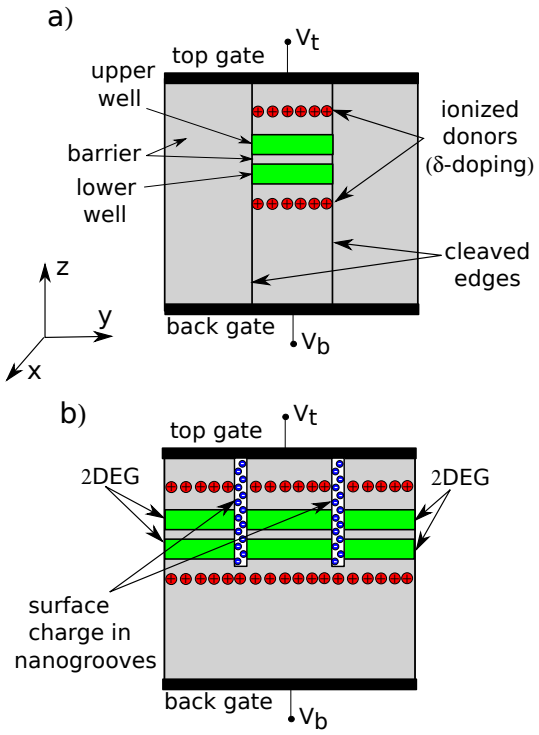

FIG. 1: (Color online) Cross section of bilayer quantum wire for: a) hard wall confinement potential as can be obtained in cleaved-edge method and b) soft lateral confinement potential due to electrons trapped on surface of the nanogrooves created with oxidization method.

The basis for fabrication of considered here two types of nanowires constitutes a two-dimensional layered lattice-matched $InP/In_{0.52}Al_{0.48}As/In_{0.53}Ga_{0.47}As$ nanostructure prepared in molecular beam epitaxy process. It consists of, going from bottom to top in the growth direction, 500 nm wide buffer, δ-doping (lower) donors layer, 25 nm barrier, two 15 nm wide quantum wells separated by thin 1 nm barrier, 25 nm wide upper barrier, second δ-doping (upper) donors layer, 20 nm wide upper buffer and on the top, 10 nm wide capping layer. For simplicity, we assume that all buffers and barrier layers are made of $In_{0.52}Al_{0.48}As$, both quantum wells and top capping layer are formed within $In_{0.53}Ga_{0.47}As$ regions. The whole structure is set on n-InP substrate that is connected to bottom back gate and another, the top gate covers the surface of the nanostructure. Due to the heavily doped substrate, the back contact is ohmic.[20] However, Schottky barrier is formed at the interface InP-InAlAs and on InGaAs-top gate contact. Therefore in calculations, we have assumed that the lower buffer directly contacts with the back gate. Cross-sections of both types of bilayer nanowires are shown in Fig.1. The height of Schottky barrier may differ much in the range $0.3 - 0.7$ V for $In_{0.53}Ga_{0.47}As$[21] and in the range $0.6 - 0.75$ V for $In_{0.52}Al_{0.48}As$[22] depending on surface roughness and material of gates. In order to remove the dependence of our results on Schottky barrier height we present them as functions of top and bottom gates voltages decreased by Schottky barrier i.e. $\Delta V_{t/b} = V_{t/b} - V_{S_{t/S_b}}$, where V_{S_t} and V_{S_b} are the Schottky barriers on the top and back contacts. In other words, $\Delta V_{t,b}$ define the shifts of conduction bands at top and bottom interfaces. The Fermi level in considered nanowire is defined by two external reservoirs of electrons that is source and drain. It is assumed to be equal $E_F = 0$ throughout this paper. The voltages applied to back and top gates do not change the Fermi level in the wire, which is established by source and drain, but may change the maximal kinetic energies in both, the upper and lower layers. We use dielectric constant $\varepsilon = 14.2$.[24] The applied conduction band offset for InGaAs/InAlAs heterojunction equals 504 meV and the electron's effective mass $m^* = 0.04m_0$. We assumed a constant value of gyromagnetic factor as for InGaAs[25] which equals $g^* = 4.0$.

On InAlAs surfaces of nanogrooves the Fermi level is pinned inside an energy gap. Following Hwang et. al.[26] we model the density of occupied states on the barrier surface by formula $D_{InAlAs} = D_1 + D_2 \cdot F_2$ with $D_1 = 3 \cdot 10^{11}\text{cm}^{-2}$ and $D_2 = 1.61 \cdot 10^{12}\text{cm}^{-2}$ being the densities of the lower and the upper energy states, respectively. The deeper surface state (D_1) is fully occupied while the occupation of the upper one (D_2) is dependent on the position of global Fermi level and actual electrostatic potential on the surface:

$$F_2 = \frac{1}{\sqrt{2\pi}\sigma_2}\int_{-\infty}^{\infty} exp\left[-\frac{\left[(E-E_F)-(V_b-V_2+V_{Poiss})\right]^2}{2\sigma_2^2}\right] f(E)dE \quad (1)$$

where $E_F = 0$ is the Fermi energy, $V_b = 504$ meV is the barrier height, V_{Poiss} is the electrostatic potential obtained as solution of Poisson equation, $V_2 = 650$ meV is the position of the upper surface state related to conduction band in InAlAs, $\sigma_2 = 13$ meV is the half-width of an upper surface state and $f(E)$ is the Fermi-Dirac distribution function. Density of surface states for InGaAs is not known, but Fermi level is pinned 300 meV above the maximum of valence band.[27] We have simplified our task and assumed that surface density is equal to $D_{InGaAs} = D_3 \cdot F_3$ with $D_3 = 3 \cdot 10^{11}\mathrm{cm}^{-2}$ and the scaling function F_3 defined in Eq.1 but with quantities V_2 and σ_2 replaced by $V_3 = 510$ meV and $\sigma_3 = 10$ meV.

B. Calculations of electronic density and conductance

In order to calculate the density and conductance in a wire for particular set of the top and back gates voltages we have adopted the method of lattice Green function described by Ando[28] and optimized by Ihnatsenka and Zozoulenko.[18] First, we discretized our problem on rectangular lattice: $x_l = l\Delta x$, $y_m = m\Delta y$, $z_n = n\Delta z$ with Δ_α ($\alpha = x, y, z$) being the distances between neighbouring mesh points in each of three dimensions. It allows us to write a tight binding Hamiltonian for our system:

$$\begin{aligned} H^\sigma_{x,y,z} &= \sum_l \sum_{m=1}^{N_y}\sum_{n=1}^{N_z} \{\, (\varepsilon_{x,y,z} + V(m,n)^\sigma)\, a^+_{lmn}a_{lmn} \\ &- (\, t_x a^+_{lmn}a_{l+1\ mn}e^{-I\lambda_{l,l+1}} \\ &+ t_y a^+_{lmn}a_{lm+1n}e^{-I\lambda_{m,m+1}} \\ &+ t_z a^+_{lmn}a_{lmn+1}e^{-I\lambda_{n,n+1}} + h.c.\,)\,\} \end{aligned} \quad (2)$$

In above equation we use the following notation: a^+_{lmn} and a_{lmn} are creation and annihilation operators defined on a lattice, $\varepsilon_{x,y,z} = 2(t_x + t_y + t_z)$ is on site energy, $t_\alpha = 1/2/m^*/(\Delta\alpha)^2$ are hopping terms for $\alpha = x, y, z$, $V^\sigma(m,n)$ is an effective potential in the wire for electrons with spin σ. Phase factors represent the Peierls shift due to vector potential $\vec{A}(\vec{r})$:

$$\lambda_{p,p+1} = \frac{e}{\hbar}\int_{\vec{R}_p}^{\vec{R}_{p+1}} \vec{A}(\vec{r})d\vec{r} \quad (3)$$

where $p = l, m, n$ defines the direction of integration when moving between two neighbouring points $(\vec{R}_p, \vec{R}_{p+1})$ on a lattice provided that the other two indices do not change. We choose the vector potential in nonsymmetric gauge $\vec{A} = [zB_y - yB_z, 0, 0]$ that gives magnetic field $\vec{B} = [0, B_y, B_z]$ which is perpendicular to direction of electron flow in a wire. Effective potential is given by $V^\sigma = V_c + V^\sigma_{xc} + g\mu B\sigma$, where V_c is the confinement potential in the nanostructure, $V^\sigma_{xc} = \frac{\partial n^\sigma \varepsilon^\sigma_{xc}}{\partial n^\sigma}$ is an exchange-correlation potential calculated within local spin density approximation[29] for three dimensional systems with Ceperley-Alder aproximation for correlation energy.[30] The last term describes the spin Zeeman factor for which we used value g=4.0 as for InGaAs.[31]

The Bloch states for free electron motion in longitudinal direction in a wire can be defined in a mixed energy and position representation formulated by Ihnatsenka and Zozoulenko[18]:

$$|\psi^\sigma_\alpha\rangle = \sum_l e^{ik^\sigma_\alpha l}\sum_{m=1}^{N_y}\sum_{n=1}^{N_z}\psi^\sigma_\alpha(m,n)a^+_{lmn}|0\rangle \quad (4)$$

$\psi^\sigma_\alpha(m,n)$ represents a wave function for y and z quantization directions. It can be expressed as linear combination of basis functions:

$$\psi^\sigma_\alpha(m,n) = \sum_{j=1}^{M} d^\sigma_{\alpha,j}\phi^\sigma_j(m,n) \quad (5)$$

Here we have modified slightly the method of Ihnatsenka and Zozoulenko[18] since we have enabled existance of two basis for spin-up and spin-down electrons. This step is particularily important in calculations for wire that has smooth lateral confinement potential which is not known at the begining and a few restarts are needed in self-consistent computations. Before each restart the recalculation of basis functions are made for better approximated effective potentials, for spin-up and spin-down electrons separately. Such conduct ensures size-consistency in our simulations and requires less basis elements needed for convergence. The basis functions $\phi^\sigma_j(m,n)$ are the eigenfunctions of two-dimensional Hamiltonian for a single slice of the wire:

$$\begin{aligned} H_{y,z} &= T_{yz} + V^\sigma \\ &= \sum_{m=1}^{N_y}\sum_{n=1}^{N_z}(2t_y + 2t_z + V^\sigma(m,n))a^+_{mn}a_{mn} \\ &- (t_y a^+_{mn}a^+_{m+1n} + t_z a^+_{mn}a^+_{mn+1} + h.c.) \end{aligned} \quad (6)$$

In case of wire with rectangular side confinement we use the same basis functions for spin-up and spin-down electrons as obtained for pure rectangular well potential $V^\sigma = V_c(m,n)$ whereas in case of wire with smooth side

confinement we calculate two separate basis functions for potential $V^\sigma = V_c + V_{xc}^\sigma + g\mu_b B$. Introducing operators for creation $c_{lj}^+ = \sum_{m,n} \phi_j(m,n) a_{l,m,n}^+$ and annihilation $c_{l,j} = (c_{l,j}^+)^+$ of basis states at any position l in a wire we may rewrite the three-dimensional Hamiltonian in the required energy and position space representation:

$$H_{xyz} = \sum_l \left\{ \sum_{j,j'}^{M} \left(T_{jj'} + V_{jj'}^\sigma \right) c_{lj}^+ c_{lj'} - \sum_{j,j'}^{M} \left(t_{jj'}^L c_{lj}^+ c_{l+1j'} + t_{jj'}^R c_{l+1j}^+ c_{lj'} \right) \right\} \quad (7)$$

The sum of kinetic and potential terms are as follows:

$$T_{jj'} + V_{jj'}^\sigma = \sum_{mn} \left[T_{yz}(mn) + 2t_x + V^\sigma(mn) \right] \phi_j(mn) \phi_{j'}(mn) \quad (8)$$

where we skipped σ index in basis functions while the element $T_{yz}(mn)$ is defined in Eq.6. The matrix elements $t_{jj'}^R$ and $t_{jj'}^L = (t_{jj'}^L)^*$ describe the coupling of two neighbouring slices l and $l+1$:

$$t_{jj'}^R = t_x \sum_{mn} \phi_j(mn) e^{I\lambda_{ll+1}} \phi_{j'}(mn) \quad (9)$$

Further procedure is identical as in the method of Ihnatsenka and Zozoulenko for strictly two-dimensional quantum wire[18], that is, we calculate Green function for a single slice, determine the Bloch states ψ_α^σ and wave vectors k_α^σ for propagating and evanescent modes for given energy. Having wave functions ψ_α^σ we used them to construct the surface Green functions of the left ($\Gamma^{L,\sigma}$) and right ($\Gamma^{R,\sigma}$) semi-infinite wires which allows finally to get the Green function $G^\sigma(mn, m'n', E)$ for the infinite bi-layer wire. For more details see work [18]. Having the Green function for infinite wire, we use a standard formula for local density of states $\rho^\sigma(mn, E) = -Im[G^\sigma(mn, mn, E)]/\pi$ and the total spin electronic density $n_e^\sigma(nm) = \int_{E_{min}}^{\infty} \rho^\sigma(nm, E) f(E) dE$. The total charge density in a system is the sum of electron density confined in the lower and upper quantum wells (n_e^σ), charge of ionized donors in the lower (n_1) and in the upper (n_2) δ-doped layers and for second type wire only, the surface charge gathered in nanogroves (n_s):

$$n_{tot} = n_e^\uparrow + n_e^\downarrow + n_s - n_1 - n_2 \quad (10)$$

We use this charge density in Poisson equation which is solved with von Neumann boundary conditions on left and right sides of the nanostructure while Dirichlet boundary conditions were used on top and bottom gates. For particular set of top and back gate voltages, the total charge density and the effective potential for considered type of lateral confinement were computed iteratively in self-consistent manner. Iterations were continued until relative change in total denisty was less than 10^{-4} what also have guaranteed convergance of effective potential. Then, the value of conductance was determined according to Landauer formula:

$$G_{cond}^\sigma = \frac{e^2}{h} \sum_\alpha \int_{E_F-6kT}^{E_F+6kT} \left(-\frac{df}{dE} \right) dE \quad (11)$$

where α indicates summation over all active transport channels for given Fermi energy. Here, we are particularly intereseted in spin polarization of a conductance. For quantitative analysis we used the following definition of spin polarization of considered quantity: $\eta_X = (X^\uparrow - X^\downarrow)/(X^\uparrow + X^\downarrow)$, where $X^\uparrow$ and $X^\downarrow$ correspond to spin-up and spin-down parts of that quantity which in our work are: the conductance G_{cond} and the total electronic density n_e in the nanowire.

The specific properties of a bi-layer wire that appear in the transverse high magnetic field depends strongly on the energy splitting between the lowest symmetric and antisymmetric states ΔE_{SAS}.[32] For low values of ΔE_{SAS}, the effects of vertical modes mixing get stronger, that is, there are developed deeper side minima in energy dispersion relation E(k).[8] Therefore, in order to monitor this quantity, for each work point i.e. the pair of confinement potential shifts ΔV_b and ΔV_t, after a self-consistency was reached, we have also determined the lowest eigenenergy and the corresponding wave function for isolated, the lower and upper wells. Diagonalization of Hamiltonian given by Eq.6 with this two member basis $\{\psi_l, \psi_u\}$ provides required energies for symmetric (E_S) and antysymmetric (E_{AS}) two-wells state provided that both wells have more or less the same shape and depth. In such case $\Delta E_{SAS} = E_{AS} - E_S$ gets its minimum. Otherwise, due to detuning of both single-well states, the value of ΔE_{SAS} grows.

III. RESULTS

A. Bi-layer nanowire with rectangular lateral confinement potential

In calculations performed for rectangular confinement potential we used following parameters: $B_y = 10$ T, $B_z = 1$ T, $\Delta_x = \Delta_y = 1$ nm, $\Delta_z = 0.5$ nm, densities of dopants in lower and in upper δ-layers were equal $\rho_1 = 3 \cdot 10^{11}\text{cm}^{-2}$ and $\rho_2 = 4 \cdot 10^{11}\text{cm}^{-2}$ while the ionization energy of dopants was set to 5 meV. All results in this and in the next section were obtained for temperature T=1 K.

Figure 2 show spin polarization of conductance (η_G), maximal kinetic energy (ΔE_{kin}) and spin polarization of total electronic density (η_ρ) for bi-layer nanowire of $y_w = 120$ nm and $y_w = 60$ nm widths. For wider wire, polarization of conductance depends on both ΔV_b and ΔV_t values but maximal value of η_G does not exceed 30% [Fig.2(a)]. Simultaneous change in top and back gates voltages along a black line, which marks the work points for which lowest energy levels in upper and in lower wells

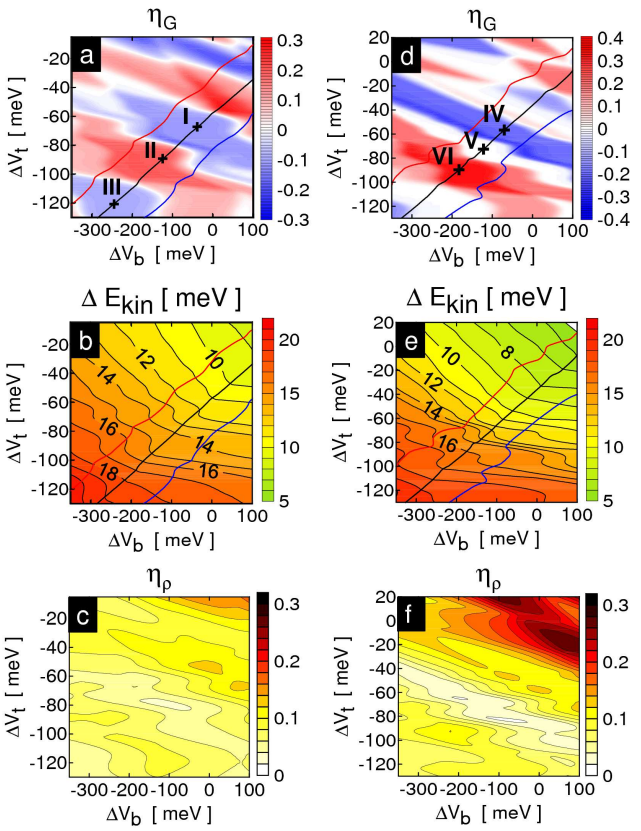

FIG. 2: (Color online) (a, d) Spin polarization of conductance, (b, e) maximum of kinetic energy and (c, f) spin polarization of total electronic density for bi-layer nanowire with rectangular lateral confinement potential and for two widths of wire: $y_w = 120$ nm (left column) and $y_w = 60$ nm (right column). Red, black and blue lines in first row indicate isolines for energy difference between the lowest energy states in upper (u) and in lower (l) wells $\Delta E_{ul} = 1, 0, -1$ meV, respectively. Crosses numbered from I to VI are work points $(\Delta V_b, \Delta V_t)$ which are analyzed in text. For work points, the energy splitting ΔE_{SAS} gets the following values: (I) 4.9 meV, (II) 4.8 meV, (III) 4.4 meV and (IV) 5.1 meV, (V) 5.0 meV, (VI) 4.9 meV.

are equal ($\Delta E_{ul} \approx 0$), makes η_G to oscillate. Sign of η_G is changed when next subband come into a transport window and due to spin Zeeman energy splitting of spin-up and spin-down $E(k)$ branches [Fig.4], positive and negative stripes lie alternately being separated by very thin unpolarized regions. What is interesting, when ΔE_{ul} is detuned and gets value of ± 1 meV [red and blue line in Fig.2], pattern of η_G does not change much besides small distortions. For the range of analyzed here values of ΔV_b and ΔV_t, maximal kinetic energy may change bewteen 9 meV and 20 meV [Fig.2(b)] with number of active subbands between 3 and 5. In our earlier work[8] we have found that for similar range of kinetic energy, spin polarization of conductance may achieve even 60%. However, those preliminary calculations were performed neglecting electrostatic interactions between electrons. In considered range of kinetic energy, polaritzation of total electronic density is low and for $\Delta E_{kin} > 10$ meV its value remains lower than 10% close to the line $\Delta E_{ul} \approx 0$. Small polarization of electron density is due to small energy splitting of spin-up and spin-down energy subbands which come into transport window alternately[see Fig.4].

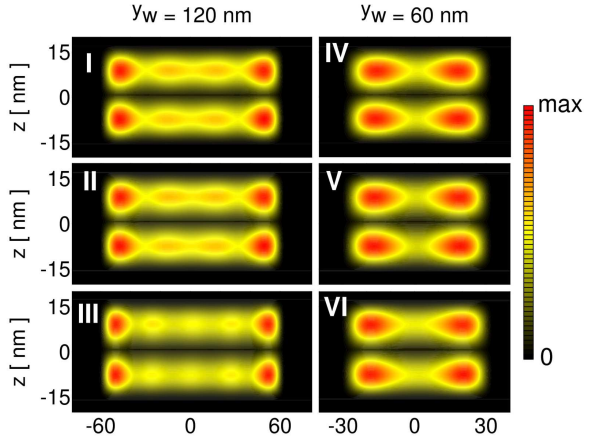

FIG. 3: (Color online) Electron densities in bi-layer quantum wire of width $y_w = 120$ nm (left column) and $y_w = 60$ nm (right column) with rectangular lateral confinement potential. Roman numbers (I-VI) correspond to work points marked in Figs. 2(a) and 2(d).

Such large divergance of results obtained within non-interacting model[8] and in the present one has forced us to analyzed this problem in detail. In figure 2(a) we have marked three arbitrarily chosen work points and number them I, II and III. Total electron densities calculated for these work points are presented in Fig.3. We notice that in each well there are developed two maximums, in the left and in the right corners. Electrons confined in wire strongly repeals each other. When they are trying to avoid other electrons they mostly localize at the edges of the system due to a lower electrostatic potential. For points I and II in Fig.3 there are two additional smaller maixmums located near the center of nanowire. When total electron density becomes larger (point III), three hardly seen smaller local maximums instead of two are developed. Similar formation of edge channels due to electron-electron interaction was predicted also for a single-layer nanowire.[19] In order to check, if the formation of edge wells can be a reason of low polarization of conductance we have repeated calculations for thinner wire which was $y_w = 60$ nm wide. Indeed, for two times thinner wire, the amplitude of conductance polarization grows up to 40% [Fig.2(d)]. Moreover, the patterns of η_g for wide and narrow wire differ qualitatively. The stripes for partly spin-up (red) and spin-down (blue) polarization are narrower with sharp edges and the unpolarized regions get wider for narrower wire. The isopotential

lines in ΔE_{kin} picture are densier in the middle part of figure 2(e) and are well correlated with the region of unpolarized total density depicted in Fig.2(f). Due to small amount of active transport channels (≤ 2) for ΔE_{kin} values less than 8 meV polarization of total density can be as large as 30%. However, the decrease of wire width has not allowed for elimination of lateral edge wells what confirms the electron densities displayed in second column of Fig.3 for work points: IV, V and VI which correspond to those marked in Fig.2(d). Although for both, wide

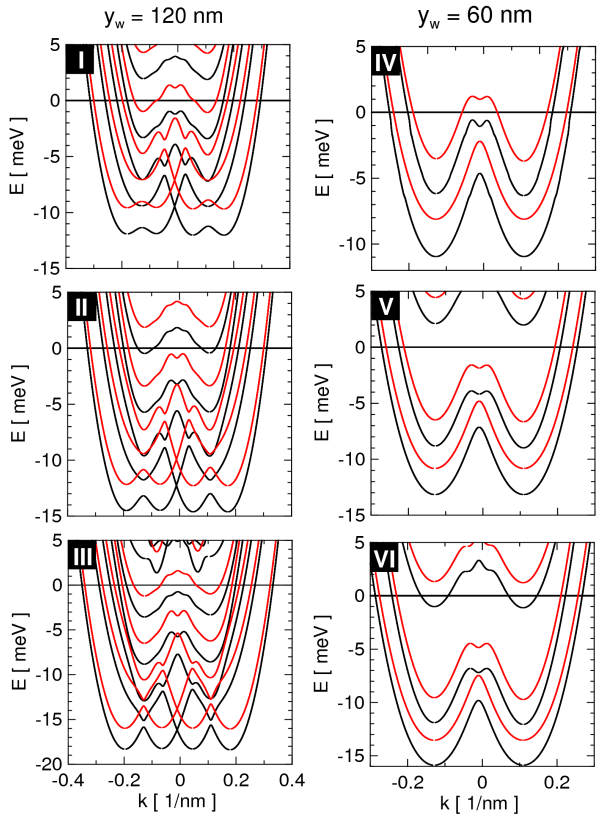

FIG. 4: (Color online) Energies of spin-up (black color) and spin-down (red color) magnetosubbands for bi-layer quantum wire of width $y_w = 120$ nm (left column) and $y_w = 60$ nm (right column) with rectangular confinement potential. Horizontal black line marks Fermi level in the system. Numbers $I - VI$ correspond to work points marked in Figs. 2(a) and 2(d).

and narrow wires, maximums of density are located at the edges, their energy subbands differ much. Energies of magnetosubbands for points I-III ($y_w = 120$ nm) and points IV-VI ($y_w = 60$ nm) are shown in Fig.4. When wire is narrow (second column), subbands have two distinct lateral minima. Two lowest subbands are separated from the upper ones what explains an appearance of large unpolarized region in η_G and in η_ρ [cf. Figs. 2(d) and 2(f)]. The shapes of magnetosubbands for narrower bi-layer wire is preserved when potentials ΔV_b and ΔV_t are decreased along the line for $\Delta E_{ul} \approx 0$. Partial polarization of conductance appears when number of Fermi level crossings with spin-up (spin-down) energy branches is larger than those for spin-down (spin-up) ones. It is easily noticable in Fig.4 for points IV and VI while for work point V the conductance is unpolarized.

Magnetosubbands for wider wire have more complicated shapes and the energy spacings between them are smaller than for narrow wire. Moreover, when depth of effective confinement potential is lowered along the line $\Delta E_{ul} \approx 0$ the shapes of few lowest subbands undergo significant modifications. The depth of two weakly marked lateral minimums in lowest subband on both sides of $k = 0$ for point I grows twice when work point is shifted to point III [cf. Figs. 4(I) and 4(III)]. During this process the lateral minimums of second subband, for $k \neq 0$, approach the maximums of the lowest subband what results in their stronger mixing. For this reason, smooth so far the energy minima and maxima now are replaced by cusps [see lower part of spin-up, first and second subbands in Fig.4(III)]. In addition, the large amplitudes of energy oscillations in vicinity of $k = 0$ make spin-up and spin-down branches to be not well separated what is the main condition for appearence of large spin polarization of conductance in bi-layer system.[8] We may thus conclude that a large spin polarization of conductance in bi-layer nanowire with hard lateral confinement can not be reached due to significant modifications of confinement potential as well as shapes of magnetosubbands.

An appearance of double lateral minumums in lowest subband can be explained in semiclassical model. For vector potential used in this paper $\vec{A} = [zB_y - yB_z, 0, 0]$, the x component of canonical wave vector ($\vec{k} = (\vec{p} + e\vec{A})/\hbar$) has the following form: $k_x = e(zB_y - yB_z)/\hbar$. The difference of k_x components of wave vectors of two electrons which move in the left and in the right edge wells lying within the same layer is $\Delta k_x = e\Delta y B_z/\hbar$. For average distance between centers of both subwells [see Fig.3] being equal $\Delta y = 100$ nm it gives wave vector shift $\Delta k_x = 0.152$ nm^{-1}. This value agrees quite well with the difference between two lateral minimums in lowest subband in Fig.4(III) for $k > 0$ or $k < 0$. For narrower wire, Δk_x has two times smaller value but due to the larger energy spacings between subsequent lateral modes [compare large energy spacings between first and second subbands in Fig.4(VI) with their smaller counterparts shown in Fig.4(III)] mixing of lateral modes is less effective what prevents the formation of two additional minimums in the lowest subband.

Splitting of the current flow into two parralel paths becomes also apparent if we look at the wave functions of first subband for $k > 0$ and kinetic energy $E_{kin} = 1$ meV (total energy is E= -17.4 meV) which are displayed in Fig.5. To get the wave function within our model, we first calculated the wave vectors k_α^σ for given energy and next used them to reduce the dimensionality of Hamiltonian given in Eq.2:

$$H_{yz}(k_\alpha^\sigma) = \langle e^{ik_\alpha^\sigma} | H_{x,y,z}^\sigma | \psi_\alpha^\sigma \rangle \qquad (12)$$

with wave functions $|\psi_\alpha^\sigma\rangle$ defined in Eq.4. Finally, the

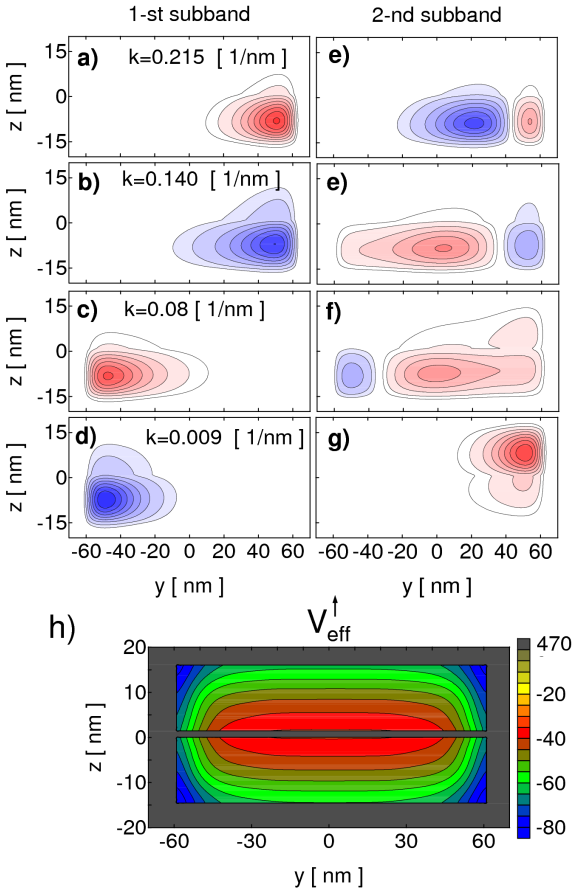

FIG. 5: (Color online) Wave functions $\psi_k^{\uparrow}(y,z)$ for first (a-d) and second (e-g) subbands calculated for rectangular confinement potential of width $y_w = 120$ nm and kinetic energy $E_{kin} = 1$ meV ($k > 0$). Wave functions are related to magnetosubbands shown in Fig.4(III). The lowest row (h) shows a cross-section of relaxed effective potential. Wave functions and effective potential were calculated for spin-up electrons.

effective two-dimensional Hamiltonian for known k_α^σ has the following form:

$$H_{yz}(k_\alpha^\sigma) = H_{yz} + \sum_{mn} \frac{1 - cos[k_\alpha^\sigma \Delta x(z\omega_y - y\omega_z)]}{m^*(\Delta x)^2} a_{mn}^+ a_{mn} \tag{13}$$

where H_{yz} is an energy operator for single slice [Eq.6] while ω_y and ω_z are the cyclotron frequencies for y and z components of $\vec{B}$. The wave functions for first and second subbands which were obtained during diagonalization of $H_{yz}(k_\alpha^\sigma)$ are shown in figures 5(a-g). All wave functions for first subband are localized in lower layer even though half of these states have negative values of group velocity $v = (\partial E/\partial k)/m^*$ [states (b) and (d)]. At first, one may think that the lowest-subband states with negative velocity should always lie in the upper layer due to action of strong magnetic force in vertical direction induced by large value of $B_y = 10$ T. However, the effective potential in both layers is not the same. Since densities of dopants in lower and in upper δ-layers differ much and due to the fact that the distance between the top gate and the upper well as well as the distance from the lower well to the back gate are different, tuning of gates voltages can not equalize the effective potentials in both layers. That is also the reason of small negative k shift in all dispersion branches shown in Figs.4 even though the depth of energy minima for $k > 0$ and $k < 0$ are at the same level. Thus, localization of wave functions for $k > 0$ or $k < 0$ for lowest subband is in slightly deeper well, independently on the direction of actual (small) group velocity. In agreement with our semiclassical explanation of quadruple energy minimums formation, one pair of wavefunctions belonging to the right most minimum [Figs.5(a,b)] are entirely localized in the lower right well while a pair of wavefunctions for second energy minimum which has lower k occupy the left one [Figs.5(c,d)]. In Fig.5(e-f) we see that the wave functions even for second subband are pinned to particular, left or right well, although these states extend over a larger area than those for first subband. For narrower wire, wave function for second subband extend more evenly over a single layer, lower or upper, what eventually prevents formation of separate energy minimums for the left and for the right edge wells.

B. Nanowire with smooth lateral confinement potential

In previous subsection we have shown that the spin polarization of conductance for bi-layer nanowire with rectangular lateral confinement potential can not reach more than 40%. It results from the fact that formation of two lateral edge wells make an electronic density to be nonhomogeneous what effectively distorts energy subbands. Therefore we repeated calculations for smooth confinement potential as can be fabricated by means of oxidization method and which is supposed to form more homogeneous electron density and in consequence shall give less distorted magnetosubbands. Calculations were performed for two nanogrooves depths: 85 nm and 115 nm. In first case, the widths of upper and lower quantum wells formed in both layers are different [see extent of electron density in nanowire in Figs.7(I-III)] since bottom of lower well lies below that of nanogroove and thus the surface charge gathered in nanogooves has less impact on lower layer than on an upper one. In the latter case, the widths of the upper and lower quantum wells become comparable [Figs.7(IV-VI)] what may influence the results. We assume that single nanogroove is $y_g = 40$ nm wide[23] and the surface states are located at its both sides. Distance between centers of nanogrooves equals 270 nm. On both sides of the nanowire in lateral direction a two-dimensional electron gas is confined in 500 nm wide channels [see Fig.1(b)]. Density of 2DEG was calculated similarily as for nanowire with an exception that

von Neumann boundary conditions were imposed on the left and on the right outermost boundaries of wave functions constituting an electron gas. To determine the surface charge gathered on nanogroove sides we have used phenomenological model provided by Hwang et. al. in work[26] and briefly described in Sec.II A. We also diversified densities of dopants in $\delta-$layers to make the electron densities confined in upper and in lower quantum wells comparable. For nanogrooves depth $h = 85$ nm we set densities of donors to $\rho_1 = 1.2 \cdot 10^{11}\text{cm}^{-2}$ (lower well) and $\rho_2 = 2.8 \cdot 10^{11}\text{cm}^{-2}$ (upper well) while for deeper nanogrooves (h=115 nm) we increase density of dopants in lower layer to $\rho_1 = 1.8 \cdot 10^{11}\text{cm}^{-2}$ and leave ρ_2 unchanged.

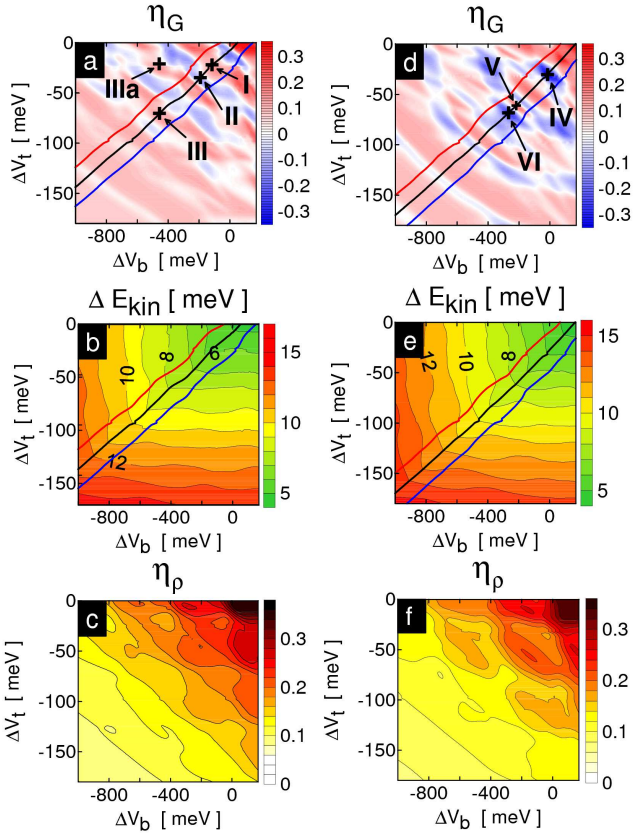

FIG. 6: (Color online) (a,d) Spin polarization of conductance, (b,e) maximum of kinetic energy and (c,f) spin polarization of total electron density for bi-layer nanowire with smooth lateral confinement potential. Depths of nanogrooves are: 85 nm (left column) and 115 nm (right column). The red, black and blue lines in first row indicate isolines for energy difference between the lowest energy states in the lower and in the upper wells $\Delta E_{ul} = 1, 0, -1$ meV, respectively. Numbers (I-VI) marks the work points $(\Delta V_b, \Delta V_t)$ which are analyzed in text.

The spin polarization of conductance and electron density confined in bi-layer nanowire as well as maximal kinetic energy as function of ΔV_b and ΔV_t are shown in Fig.6. We notice that values of η_G do not exceed 33% for both nanogroove depths. It is not however an effect of

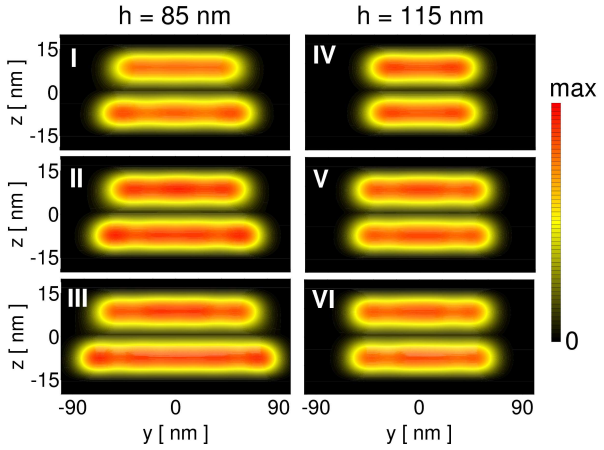

FIG. 7: (Color online) Electron densities in bi-layer quantum wire with smooth lateral confinement potential. Nanogrooves widths are: 85 nm (left column) and 115 nm (right column). Roman numbers (I-VI) correspond to work points marked in Figs.6(a,d).

granularity of electron density. Densities shown in Fig.7 for arbitrarily chosen three work points have in both cases distinct maximums which are smooth and elongated in y direction. An unexpected low spin polarization of conductance can not be also an effect of detuning the energy ladders in both quantum wells since densitites that have been obtained for deeper nanogroves are almost the same in both layers what excludes such possibility.

It is interesting that the lines of constant kinetic energy ΔE_{kin} in Fig.8(b,e) resemble a rectangle corner. When value of ΔV_b (ΔV_t) is fixed and ΔV_t (ΔV_b) is increased then the value of kinetic energy varies slightly. It results from fact that upper and lower quantum wells are strongly coupled only to one, top or back gate. For example, the change of top gate voltage from work point III to IIIa in Fig.6(a) make an energy shift in these parts of magnetosubbands which describe an electron motion in upper layer [left part of energy spectrum in Fig.8(IIIa)] leaving simultaneously an electron motion in lower layer unchanged [right part in Fig.8(IIIa)]. This strong and selective coupling results from screening properties of an electron gas which is confined at both sides of nanowire [see Fig.1(b)]. Variations of voltages applied to top (back) gate make an upper quantum well deeper or shallower what implies additional charge flow between an upper (lower) layer and external reservoirs of electrons. This effect was insignificant in nanowire with rectangular confinement potential since the electron density gathered only in nanowire can not screen much wider metallic gates. Therefore, variations of kinetic energy in Figs. 2(b) and 2(e) have such irregular patterns unlike these visible in Figs. 6(b) and 6(e).

Energy spectra calculated for work points I-VI lying on a line $\Delta E_{ul} \approx 0$ and marked in Fig.6(a,d) are presented in Fig.8. For nanogrooves depth h=85 nm, the

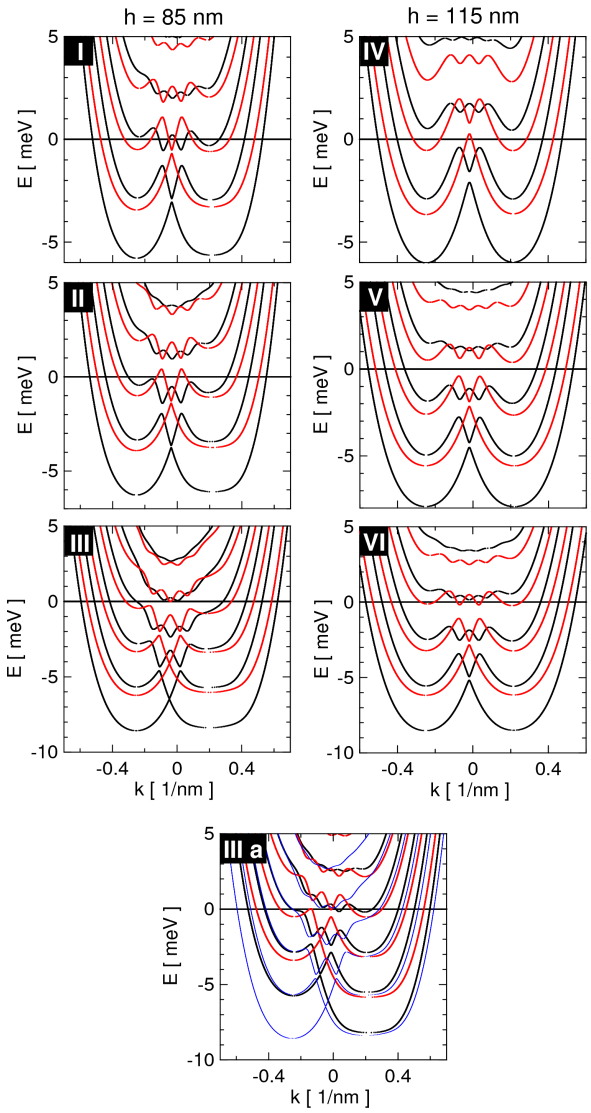

FIG. 8: (Color online) (Color online) Spin-up (black color) and spin-down (red color) energy dispersion for the bilayer quantum wire soft wall confinement potential. Horizontal black line marks the Fermi level in the system. Numbers I, II, III and IIIa correspond to work points marked in Fig.6(a) while numbers IV, V and VI correspond to those on Fig.6(d). Blue color energy branches in case IIIa are the copies of spin-up (black) branches taken from work point III for comparison only.

lower layer in nanowire is not completely surrounded by nanogrooves as it is for the upper layer. For this reason, the energy branches for $k < 0$ differ from these for $k > 0$. In Fig.8(I-III) we notice, that energy branches describing mainly the motion of electrons in the lower well (right part) are wider than these for the upper one (left part). For deeper nanogooves ($h = 115\ nm$) both nanowire layers interacts electrostatically with the surface charge in similar manner. The widths of the upper and lower wells are the same [Fig.7(IV-VI)] what translates into almost perfect mirror symmetry of energy subbands. Independently of the depth of nanogrooves, the three lowest spin-down branches (red color) are shifted up on energy scale due to spin Zeeman effect but localize near subsequent upper spin-up subbands (black color). This is a main reason of low spin polarization of conductance in nanowire with smooth confinement potential. Although, the amplitudes of oscillations in $E(k)$ in the vicinity of $k = 0$ seems to be optimal for high polarization of conductance[8] because the energy oscillations in two neighbouring subbands are separated. But actually due to frequent overlapping of opposite spin magnetosubbands at Fermi energy level, spin polarization stays low. For the same reason, polarization of the total electronic density confined in bi-layer wire is low besides a region with small values of ΔV_b and ΔV_t [upper right part in Fig.6(c,f)] when only two spin-up and one spin-down subbands cross Fermi level.

Value of gyromagnetic factor in InGaAs material that constitutes quantum wells is dependent on voltages applied to gates[31] what is omitted in our model. But, if we reasonably assume, it may change in the range $g = 3.5 - 4.2$ then the energy shift due to spin Zeeman splitting[33] varies between 2.03 meV and 2.43 meV (for $g = 4$ is equal 2.31 meV). Thus, the variations of g values induced by the changes of voltages applied to the metallic gates are too small to significantly draw aside the spin-up and spin-down subbands shown in Fig.8(I-VI). It seems, the only way to get a large spin polarization of conductance is to tune the magnetic field, especially value of B_y as it gives the main contribution to B. However, the change of magnetic field may distort much the shapes of magnetosubbands and in such case an additional tuning of both, top and back gate voltages could be required.

IV. CONCLUSIONS

We have calculated the conductance of bi-layer nanowire in tilted magnetic field taking into account an electrostatic interaction between electrons in nanosystem and for two types of lateral confinement potential: smooth and rectangular. Our considerations have mainly been focused on spin polarization of conductance which can achieve even 60% for moderate Fermi energy if interaction is neglected. Simulations were performed for wide range of voltages applied to top and back gates which allow to change the Fermi energy in lower and in upper quantum well. It was shown that in nanowire with rectangular lateral confinement potential, maxima of electron density are located at side edges of wire. If nanowire is wide then the lowest subband and the main part of second subband are localized in the same edge well. In such case, there appear two additional energy minimums in lowest magnetosubband. Independenlty of width of rectangular bi-layer wire, pseudogaps are opened in energy spectrum but due to large distortions of magnetosubbands only a moderate ($\leq 40\%$) spin polarization of con-

ductance can be reached. If lateral confinement potential in wire is smooth, local maxima in electron density are diminished and since the edge states dissappear, magnetosubbands are less distorted. Even though, the widths of pseudogaps are optimal for large spin polarization, in some cases it can not be reached due to an overlap of spin-up and spin-down magnetosubbands. Such overlap is accidental and results from spin Zeeman energy shift of spin-up and spin-down energy subbands. We may thus conclude, that in bi-layer nanowire with smooth lateral confinement potential, the large spin polarization of conductance can be achieved only if both, the magnetic field and the Fermi energies in upper and lower layers of wire will be simultaneously tuned.

Acknowledgements

The work was financed by Polish Ministry of Science and Higher Education (MNiSW)

* Electronic address: chwiej@fis.agh.edu.pl

[1] K. J. Thomas, J. T. Nicholls, M. Y. Simmons, W. R. Tribe, A. G. Davies, M. Pepper, Phys. Rev. B 59, 12252 (1999)
[2] S. F. Fischer, G. Apetrii, U. Kunze, D. Schuh, G. Abstreiter, Phys. Rev. B 71, 195330 (2005)
[3] D. Huang, S. K. Lyo, K. J. Thomas, M. Pepper, Phys. Rev. B 77, 085320 (2008)
[4] L. G. Moroukh, A. Y. Smirnov, S. Fischer, Appl. Phys. Lett. 90, 132108(2007)
[5] S. K. Lyo, J. Phys.: Condens. Matter 8, L703 (1996)
[6] J.-R. Shi, B.-Y. Gu, Phys. Rev. B 55, 9941(1997)
[7] S. K. Lyo, Phys. Rev. B 60, 7732(1999)
[8] T. Chwiej, arXiv:1508.05793
[9] A. C. Mehta, C. J. Umrigar, J. S. Meyer, H. U. Baranger, Phys. Rev. Lett. 110, 246802(2013)
[10] C. Reichhardt, C. Bairnsfather, C. J. Olson Reichhardt, Phys. Rev. E 83, 061404(2011)
[11] S. Kumar, K. J. Thomas, L. W. Smith, M. Pepper, G. L. Creeth, I. Farrer, D. Ritchie, G. Jones, J. Griffiths, Phys. Rev. B 90, 201304(2014)
[12] J. E. Galván-Moya, K. Nelissen, F. M. Peeters, Phys. Rev. B 86, 184102(2012)
[13] M. Yamamoto, H. Takagi, M. Stopa, S. Tarucha, Phys. Rev. B 85, 041308(2012)
[14] M. Huber, M. Grayson, M. Rother, W. Biberacher, W. Wegscheider, and G. Abstreiter, Phys. Rev. Lett. 94, 016805 (2005)
[15] G. Apetrii, S. F. Fischer, U. Kunze, D. Schuh, G. Abstreiter, Physica E 22, 398 (2004)
[16] A. Mühle, W. Wegscheider and R. J. Haug, Appl. Phys. Lett. 91, 133116 (2007)
[17] A. Mühle, W. Wegscheider and R. J. Haug, Appl. Phys. Lett. 92, 013126 (2008); L. Meier, A. Fuhrer, T. Ihn, K. Ensslin, W. Wegscheider, and M. Bichler Phys. Rev. B 69, 241302(R) (2004)
[18] S. Ihnatsenka and I. V. Zozoulenko, Phys. Rev. B 73, 075331 (2006)
[19] S. Ihnatsenka and I. V. Zozoulenko, Phys. Rev. B 74, 075320 (2006)
[20] A.G. Baca, F. Ren, J.C. Zolper, R.D. Briggs, S.J. Pearton, Thin Sol. Films 308, 599(1997)
[21] L. He, M. J. Costello, K. Y. Cheng, D. E. Wohlert, J. Vac. Sci. Technol. A 16, 1646 (1998)
[22] Y. Zhu, Y. Ishimaru, N. Takahashi, M. Shimizu, J. Appl. Phys. 80 (3), 1617 (1996)
[23] B. Klehn, S. Skaberna, U. Kunze, Superlattice. Microst. 25, 473 (1999)
[24] E. Diez, Y. P. Chen, S. Avesque, M. Hilke, E. Peled, D. Shahar, J. M. Cerver, D. L. Sivco and A. Y. Cho, Appl. Phys. Lett. 88, 052107 (2006)
[25] M. Dobers, J. P. Vieren, Y. Guldner, P. Bove, F. Omnes, and M. Razeghi Phys. Rev. B 40, 8075(R) (1989)
[26] J. S. Hwang, W. C. Hwang, C. C. Chang, S. C. Chen and Y. T. Lu J. Appl. Phys. 89, 396 (2001)
[27] W. Melitz, J. Shen, S. Lee, J. S. Lee, A. C. Kummel, R. Droopad, E. T. Yu, J. Appl. Phys. 108, 023711(2010)
[28] T. Ando, Phys. Rev. B 44, 8017(1991)
[29] J. P. Perdew, A. Zunger, Phys. Rev. B 23, 5048 (1981)
[30] D. M. Ceperley, B. J. Alder, Phys. Rev. Lett. 45, 566 (1980)
[31] M. Dobers, J. P. Vieren, Y. Guldner, P. Bove, F. Omnes, M. Razeghi, Phys. Rev. B 40, 8075(1989)
[32] S. F. Fischer, G. Apetrii, U. Kunze, D. Schuh, G. Abstreiter, Phys. Rev. B 74, 115324 (2006)
[33] Another contribution to energy shift of spin-up an spin-down subbands gives the exchange-correlation potential. This type of energy splitting also depends on gyromagnetic value since the larger g is, the larger difference between spin-up and spin-down densities we get.